Desalination and Water Treatment
www.deswater.com

doi: 10.5004/dwt.2017.20541

71 (2017) 406–419
April

Photocatalytic degradation of Eriochrome Black-T by the Ni:TiO_2 nanocomposites

Azad Kumar*, Gajanan Pandey

Department of Applied Chemistry, School for Physical Sciences, Babasaheb Bhimrao Ambedkar University (A Central University), Lucknow 226025, India, email: kumarazad20@gmail.com (A. Kumar)

Received 18 July 2016; Accepted 29 January 2017

ABSTRACT

Conventional chemical, biological and adsorption treatments have been applied for the removal of dyes from textile wastewater, but these processes are insufficient in removing dye contaminants. Photocatalysis is greener approach for the degradation of harmful dye pollutant compounds completely. In the present study, TiO_2 and Ni:TiO_2 nanoparticles were prepared and their photocatalytic activity was measured against Eriochrome Black-T (EBT). The photodegradation of EBT was investigated in the different conditions of concentration and pH in the presence of TiO_2 and Ni:TiO_2. The photocatalysts were characterized by X-ray diffraction (XRD), scanning electron microscope (SEM), energy-dispersive X-ray spectroscopy, UV–Vis and Brunauer -Emmett -Teller. The XRD confirmed the presence of anatase and rutile phase in the prepared photocatalysts. The Scherrer's calculations are used to determine the average particle size. The average particle size was found as 72 and 16 nm for TiO_2 and Ni:TiO_2, respectively. The SEM and transmission electron microscopy images also confirmed the formation of nanoparticles in the range of ~100 nm. The band gap energy of TiO_2 and Ni:TiO_2 was calculated by talc plot and obtained as 3.2 and 3.0 eV, respectively. The photocatalyst activity was measured by varying pH and concentration of dye solution. Kinetics study was also performed in this investigation.

Keywords: Photocatalyst; Nanocomposites; Eriochrome Black-T; Photodegradation

1. Introduction

Nowadays water pollution has become a major threat to living organism because large amount of hazardous industrial wastes containing dyes, pigments, pharmaceutical products, industrial chemicals and various organic compounds are dumped into water bodies, causing water pollution. Since these wastes are stable to light, oxidizing agents and resistant to aerobic digestion; therefore, pose serious ecological problems [1–4]. Some investigations reported that approximately 12% of the synthetic textiles dyes use each year, such as Caramine, Indigo Red, Red 120, Rhodamine B, Methylene Blue and Eriochrome Black-T (EBT) [5–8], while 20% of these dyes are lost during manufacturing and processing operations, which enter into water through effluents. While conventionally chemical [9], biological [10] and adsorption [11] treatments have been applied for the removal of dyes from industrial wastewater but these processes are insufficient in removing dye contaminants [12–15].

Photodegradation is an advanced oxidation process and it has lot of advantages over traditional wastewater treatment techniques such as chemical oxidation [16], activated carbon adsorption [17], biological treatment [18], etc. Activated carbon adsorption method involves the phase transfer of pollutants without decomposition and thus creates another pollution problem. Chemical oxidation method is unable to remove all organic substances and it is suitable for the removal of pollutants at high concentrations. The biological treatments are very slow, dispose large amount of sludge and required strict control of proper pH and temperature [19]. In this regard, photocatalytic processes have advantages for the removal of pollutants even at

* Corresponding author.

low concentration for industrial wastewater [20]. Moreover in photooxidation, complete oxidation of organic pollutants take place within few hours, even at parts per billion level, without formation of secondary hazardous products using highly active and cheap catalysts which can be used in specially designed reactor systems [21].

Titanium dioxide is a widely accepted photocatalyst due to its high oxidation efficiency, non-toxicity, high photostability, chemical inertness and environmentally friendly nature [22–24]. It is a wide band gap (~3.2 eV) semiconductor and mineralizes a large range of organic pollutants such as herbicides, dyes, pesticides, phenolic compounds, tetracycline, sulphamethazine, etc., under UV irradiation [25]. In photocatalytic processes, the photon with energy equal to or greater than the energy gap (3.2 eV) is absorbed by TiO_2 particles; therefore, holes (h^+) are created in the valence band (VB) and electrons (e^-) in the conduction band (CB), which diffuses to the surface of TiO_2 and participates in redox reactions of the adsorbed substrates [26].

TiO_2 is a large band gap semiconductor; therefore, it is suitable in UV light photodegradation. Since the solar light contains only 5% UV radiation; therefore, TiO_2 is not suitable photocatalyst in solar light. Further electron hole recombination is another drawback in TiO_2 mediated photocatalysis. The above drawbacks could be overcome at some extent by doping metal ions in TiO_2 host [27–29]. In the present investigation, Ni^{2+}-doped TiO_2 has been performed in a green synthetic manner and its photocatalysis activity has been performed against EBT.

2. Experimental setup

2.1. Materials

The materials used in this study were purchased from Merck, India. All chemicals used in this investigation namely titanium tetrachloride, sodium hydroxide, ammonia, nitric acid and EBT dye are analytical grade reagent and used as supplied. Ethyl alcohol and deionized water were used as solvents in this experiment.

2.2. Synthesis of TiO_2

In this method, both $TiCl_4$ solution (200 g/L) and NaOH solutions (64.5 g/L) were added dropwise to water with stirring. When pH of resulting solution reaches to 7, slurry was formed which was filtered. The filter cake of TiO_2 was washed and redispersed in water to prepare 1 M of TiO_2 slurry. TiO_2 slurry was added to an aqueous solution of HNO_3 and resulting solution was refluxed for 2 h at 95°C, cooled naturally to room temperature, neutralized with 28% of aqueous ammonia, filtered, washed with double distilled water and calcined at 400°C. The TiO_2 was formed as follows [30]:

$$TiCl_4 + 4NaOH + NH_3 \rightarrow Ti(OH)_4 + 4NaCl \quad (1)$$

$$Ti(OH)_4 \rightarrow TiO_2 + 2H_2O \quad (2)$$

2.3. Synthesis of Ni-doped TiO_2 (Ni:TiO_2)

5 g of as-prepared TiO_2 was dissolve in 100 mL water:alcohol (ratio 3:1 v/v) mixture. 5% alcoholic nickel acetate solution was added dropwise to TiO_2 solution. The dispersion was agitated continuously for 4 h at 80°C. After the treatment, the residue was removed by filtration and sintered for 1 h in the presence of air at 400°C, keeping in a silica boat inside muffle furnace. After sintering, slow annealing was done at room temperature. Content was taken out from furnace and stored in closed air tight bottles. The obtained yield of prepared nanocomposites of TiO_2 and Ni:TiO_2 was <90% of the expected theoretical yield [31].

$$TiO_2(Soln) + Ni(CH_3COO)_2(alc\ sol) \rightarrow Ni{:}TiO_2 \quad (3)$$

2.4. Characterization

X-ray diffraction (XRD) pattern of above synthesized TiO_2 and Ni:TiO_2 was recorded on X-ray diffractometer (Bruker AXS D8 Advance System, Germany). The particles morphology of the photocatalysts were studied using scanning electron microscope (SEM; JEOL JSMn 6490 LV). The surface area and pore characteristics of the derived photocatalyst were determined by nitrogen adsorption/desorption isotherms at 77 K (boiling point of nitrogen gas at 1 atm pressure) using a Brunauer -Emmett -Teller (BET) surface area analyzer (BELSORP-max, Japan). Since the absorption of light by photocatalysts and their band gap average energy are the most crucial step in any photocatalyzed reaction, the UV–visible spectra of material were recorded on spectrophotometer (UV 2450, Shimadzu, Japan). The Fourier transform infrared (FTIR) spectra of the pellets were recorded using a FTIR spectrometer from Thermo Scientific, India (Nicole 6700). For FTIR study, the photocatalyst (2 mg) was mixed with 200 mg of KBr and then made into pellets.

2.5. Photodegradation of EBT

The photocatalytic activity of as-prepared TiO_2 and Ni:TiO_2 materials was evaluated by photodegradation of EBT (structure shown in Fig. 1) under visible light which is <420 nm using a filter (fluorescent visible lamp, 500 W, Philips, Maharashtra, India) exposure in a photocatalytic chamber. 200 mg photocatalyst was dispersed in 20 mL of solution of EBT dye of different concentration (16.6×10^{-5}, 20.0×10^{-5}, 25.0×10^{-5} and 33.3×10^{-5} M), in the dark condition for 30 min in order to achieve the adsorption equilibrium. The solution was irradiated continuously by visible light in a photocatalytic chamber. During irradiation, solution was agitated using a magnetic stirrer and air was bubbled into the reaction medium to provide a constant supply of oxygen. After desired time interval, an aliquot of solution was isolated, centrifuged and its absorbance was measured using UV–visible spectrophotometer to calculate the percentage degradation. The photocatalytic degradation efficiency was calculated using the following equation [32,33]:

$$(\%)\text{Degradation} = \frac{A_o - A}{A_o} \times 100 \quad (4)$$

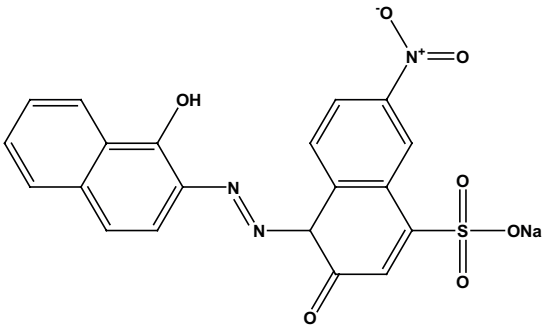

Fig. 1. Molecular structure of EBT.

where A_o the initial absorbance of the dye solution and A is the absorbance after irradiation at particular time.

2.6. GC–MS analysis

In order to observe the products of photocatalytic experiment gas chromatography–mass spectroscope (GC–MS) analysis (Shimadzu, GC-2010 and GC-MS-QP 2010 plus, using RTX-5Sil-MS column [30 m × 0.25 mm × 0.25 μm]) was carried out. In a typical experiment, 5 mL of EBT solution was collected after 180 min of UV-light exposure in the presence of catalyst. The solutions were centrifuged (5,000–8,000 rpm), filtered through cellulose filter (0.22 μm) and extracted in three successive quantities (5 mL) of ethyl acetate. The ethyl acetate extract carry samples were passed through sodium sulphate (anhydrous), evaporated to dryness over rota-evaporator and their traces removed over gentle stream of N_2 gas. Residue thus obtained redissolved in methanol (GC grade) and analyzed. Helium was used as a carrier gas with a flow of 1 mL/min through capillary column. Injector was maintained at 240°C, while transfer line was kept at 260°C and 1 μL of the sample was injected. Oven was programmed at 60°C–300°C at 6°C/min rise of temperature [34].

3. Results and discussion

3.1. Powder X-ray diffraction analysis of TiO_2 and Ni:TiO_2

The XRD pattern of as-prepared TiO_2 and Ni:TiO_2 nanoparticles is depicted in Figs. 2(a) and (b). In the XRD pattern of TiO_2, the major peaks observed at 2θ value 25.2°, 37.2°, 48.3° and 55.4° are corresponds to anatase phase whereas the peaks at 26.9°, 28.2°, 42.6° and 54.2° indicate the presence of rutile phase. In the XRD pattern of Ni:TiO_2, intensity of peaks decreased compared with TiO_2. This is due to change in crystallinity, grain fragmentization and partial amorphization. The observed X-ray diffractogram of samples was analyzed further to estimate average grain size in the sample using Scherrer's equation [35]:

$$T = \frac{K\lambda}{\beta\cos\theta} \quad (5)$$

where T is the mean size of the ordered (crystalline) domains, which may be smaller or equal to the grain size, K is a dimensionless shape factor, with a value close to unity. The shape factor has a typical value of about 0.9, but varies with the actual shape of the crystallite, λ is the X-ray wavelength, β is

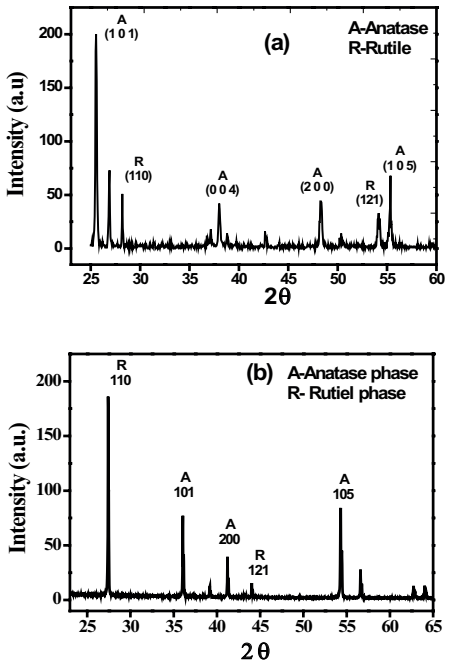

Fig. 2. Observed XRD pattern of: (a) TiO_2 and (b) Ni:TiO_2.

the line broadening at half the maximum intensity (full width at half maximum), (in radians) and θ is the Bragg angle. The particle size of TiO_2 and Ni:TiO_2 was calculated as 72 and 16 nm, respectively, using above equation.

3.2. Scanning electron microscope

The morphology of the samples was investigated by scanning electron microscopy analysis. Fig. 3 clearly shows that both the prepared samples are obtained as agglomerate in nanometric dimension. The doping of Ni^{2+} ion indicates that the particle size reduces due to the penetration of nickel in the lattice of titanium dioxide.

3.3. Transmission electron microscopy

Transmission electron microscopy (TEM) analysis of materials was used to examine the crystallite/particle size morphology. The prepared TiO_2 powders consist of both spherical and semispherical shape, on the contrary, the particles of Ni:TiO_2 have mostly spherical morphology.

It can be estimated that the particle size of TiO_2 and Ni:TiO_2 powders in Figs. 4(a) and (b) are in the nanoscale with the grain size <100 nm.

3.4. Surface area analysis (BET)

The specific surface area, pore volume and average pore size of the TiO_2 and Ni:TiO_2 photocatalyst were determined by N_2 adsorption technique using BET. Fig. 5(a) shows adsorptions' desorption and Fig. 5(b) Barrett -Joyner -Halenda (BJH) plot and Table 1 summarizes their physical properties. The TiO_2 modified by Ni^{2+} incorporation during thermal treatment, lead to a marked increase of the BET surface areas, average pore radius and pore volume. Doping with 5% Ni, the crystallite

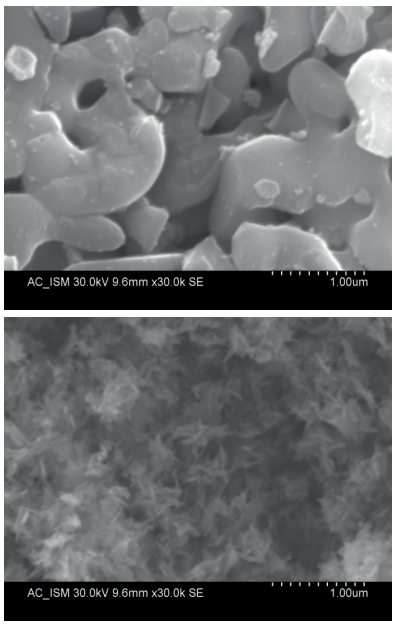

Fig. 3. Observed SEM pattern of: (a) TiO_2 and (b) Ni:TiO_2.

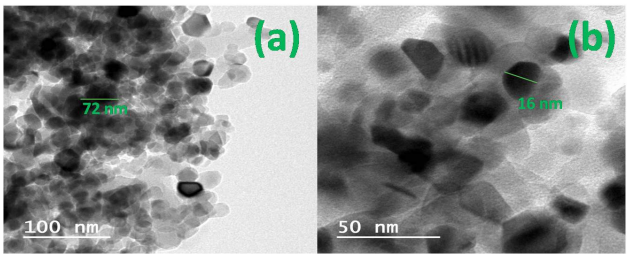

Fig. 4. Observed TEM pattern of: (a) TiO_2 and (b) Ni:TiO_2.

size was decreased and the surface area value increased. These results suggest that Ni doping effectively inhibits TiO_2 grain growth probably by staying at grain boundaries thereby decreasing the crystallite size and increasing the surface area. The decrease in grain growth can also be attributed to the formation of Ni–O–Ti bonds in the doped powders, which inhibits the growth of the TiO_2 crystals.

3.5. UV–Vis spectra

Aqueous suspensions of the samples were used for the UV absorption studies. The UV -Vis spectra are shown in Figs. 6(a) and (b). The absorption spectrum of TiO_2 consists of a single broad intense absorption between 250 and 300 nm due to the charge transfer from the VB to the CB [36]. The undoped TiO_2 showed absorbance in the shorter wavelength region while Ni:TiO_2 result showed slight red shift in the absorption edge.

The doping of Ni ions into TiO_2 could shift optical absorption edge from UV to visible range, but no prominent change in TiO_2 band gap was observed [37,38].

3.6. Band gap energy determination

The band gap of samples was calculated by extrapolation of the $(\alpha h\nu)^2$ vs. $h\nu$ plots, where α is the absorption coefficient

Table 1
BET data of TiO_2 and Ni:TiO_2

Sample	Surface area (m^2/g)	Pore volume (cm^3/g)	Pore radius (nm)
TiO_2	2.1522	10.132×10^{-3}	1.21
Ni:TiO_2	46.685	9.5124×10^{-2}	1.64

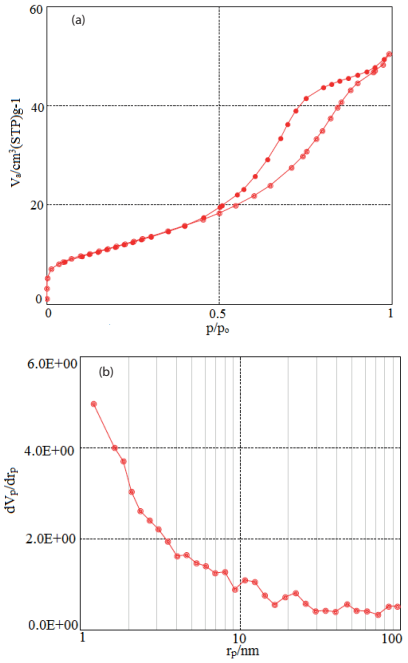

Fig. 5. (a) Adsorption–desorption plot of Ni:TiO_2 and (b) BJH plot of Ni:TiO_2.

and $h\nu$ is the photon energy, $h\nu = (1{,}239/\lambda)$ eV. The value of $h\nu$ extrapolated to $\alpha = 0$ gives an absorption energy, which corresponds to a band gap (E_g). Figs. 7(a) and (b) yield an E_g value of 3.2 eV for TiO_2 and 3.0 for Ni:TiO_2 [39]. The slight decrease in band gap energy in case of Ni:TiO_2 is due to the formation of sub-band level between VB and CB caused doping of Ni^{2+} in TiO_2 host.

3.7. FTIR spectroscopy

FTIR spectra of undoped and 5% Ni-doped TiO_2 samples (Fig. 8) show peaks corresponding to stretching vibrations of the O–H and bending vibrations of the adsorbed water molecules around 3,350–3,450 and 1,620–1,635 cm^{-1}, respectively. The broad intense band below 820, 804, 592 and 456 cm^{-1} is due to Ti–O–Ti vibrations. The shift to the higher wave numbers and sharpening of the Ti–O–Ti band may be due to decrease in size of the catalyst nanoparticles. In addition, the surface hydroxyl groups in TiO_2 increased with the increasing of Ni loading, which is confirmed by increase in intensity of the corresponding peaks. The FTIR spectra of Ni:TiO_2 show strong band at 1,075 cm^{-1}, corresponds to the vibration of Ni–O bond and confirms the penetration of nickel in titania [40].

4. Photodegradation of EBT

The photocatalytic degradation of EBT has been studied in the presence of TiO_2 and Ni:TiO_2 nanoparticles. Different concentration solutions of dye were prepared in 3:2 (v/v) ratio of water and alcohol. The known amount of photocatalyst 0.2 g was dispersed in the 20 mL dye solution and the reaction mixture was irradiated with visible light with constant stirring on magnetic stirrer. After different time interval, an aliquot of solution was separated, centrifuged and absorption was recorded spectrophotometrically. The results obtained for the degradation of EBT are shown in Fig. 9. As obvious from the graph, the percentage removal of dye decreases with increase in concentration. Further, the photocatalytic efficiency of TiO_2 increases by doping Ni^{2+} ion in TiO_2 host. The photodegradation efficiency of Ni:TiO_2 is greater than bare TiO_2 [41,42].

4.1. Effect of dye concentration

The effect of dye concentration on photocatalytic degradation was studied in the presence of TiO_2 and Ni:TiO_2 materials, keeping the amount of catalyst constant. Known concentration of dye solution was prepared in water:alcohol (3:2, v/v) ratio. The known amount of photocatalyst (0.2 g) was dispersed in the different concentration of dye (33.3×10^{-5}, 25.0×10^{-5}, 20.0×10^{-5} and 16.6×10^{-5} M) and reaction mixtures were irradiated by visible light. The effect of photocatalytic degradation with time was measured and result is shown in Fig. 9. When the concentration of solution increased, the number of dye molecule also increased, therefore, the effective number of photon penetrating the dye reached at the catalyst surface also reduced, owing to hindrance in the path of light, thereby reducing the reactive hydroxyl and superoxide radicals and decreasing the percentage degradation [43].

4.2. Effect of pH

The photodegradation reaction was also carried out under varying pH conditions from 2 to 9, by addition of H_2SO_4 and NaOH, keeping other parameters same. The results (Fig. 10) show that degradation of dye is highest in acidic medium (at pH = 2) while it decrease with increase in pH and ultimately becomes constant after pH 7. This implies that acidic condition is favourable for formation of the reactive intermediate hydroxyl radicals. This further helps in enhancing the reaction rate. On the other hand in neutral condition the formation of reactive intermediate is relatively less favourable and hence not feasible [44].

4.3. Effect of photocatalyst

It is clear from the results shown in Figs. 9 and 10 that both TiO_2 and Ni:TiO_2 are effective photocatalyst for degradation of EBT dye, however, Ni:TiO_2 seems to be more effective photocatalyst for degradation of EBT.

4.4. Effect of dose of photocatalyst on photodegradation of EBT

The effect of photocatalyst dose on the photodegradation of EBT was studied by applying the different concentrations (200, 100 and 50 mg/L) of the photocatalyst shown in Fig. 11. The degradation rate of EBT was found to increase by increasing the dose of photocatalyst from 50 to 200 mg/L. This is due to increase in the active site on the surface of the photocatalyst. When the Ni is incorporated in TiO_2, the band gap energy is decreased which enhanced the photoefficiency, the surface area of photocatalyst also increased the efficiency of photocatalyst.

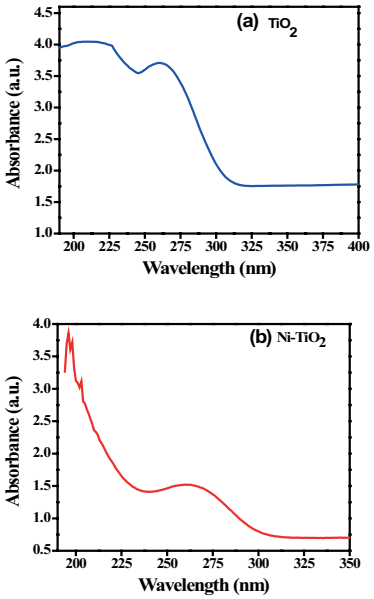

Fig. 6. UV spectra of: (a) TiO_2 and (b) Ni:TiO_2.

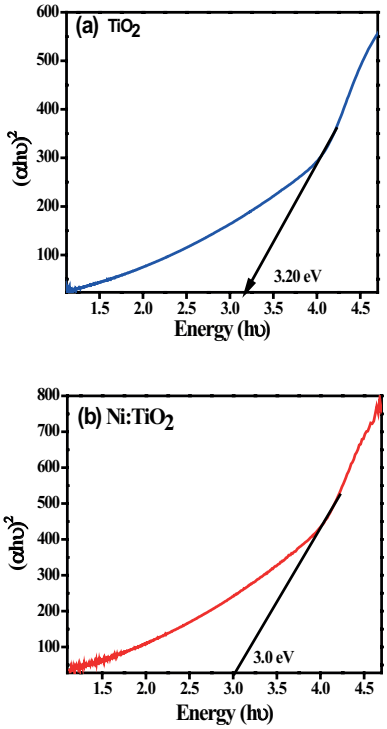

Fig. 7. Band gap energy of: (a) TiO_2 and (b) Ni:TiO_2.

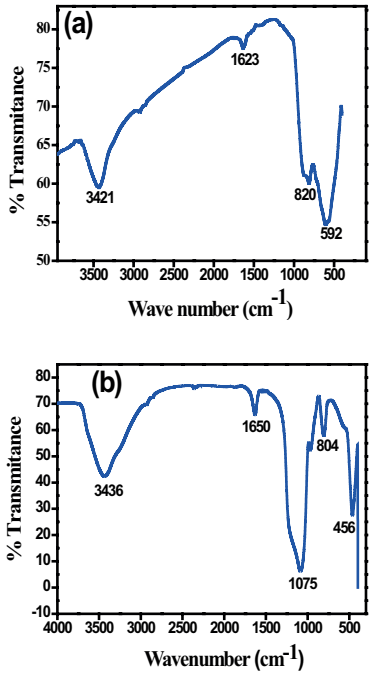

Fig. 8. FTIR spectra of: (a) TiO_2 and (b) Ni:TiO_2.

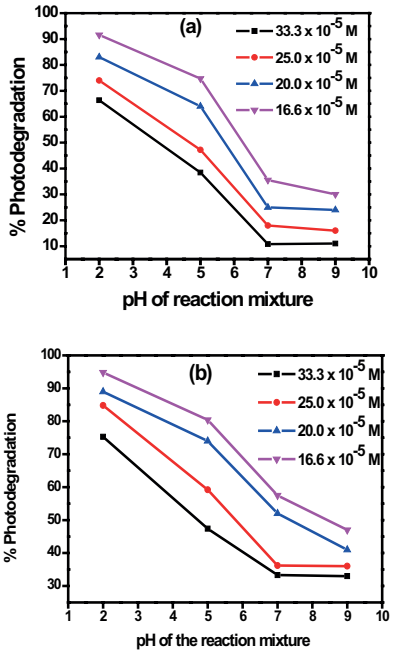

Fig. 10. Effect of pH on photodegradation of EBT at various concentrations: (a) TiO_2 and (b) Ni:TiO_2.

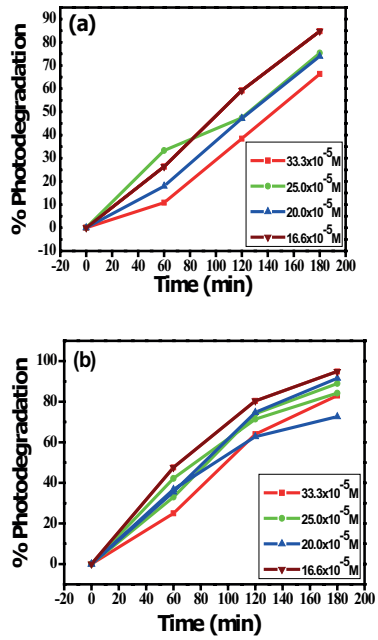

Fig. 9. Photodegradation of EBT at different concentration: (a) TiO_2 and (b) Ni:TiO_2.

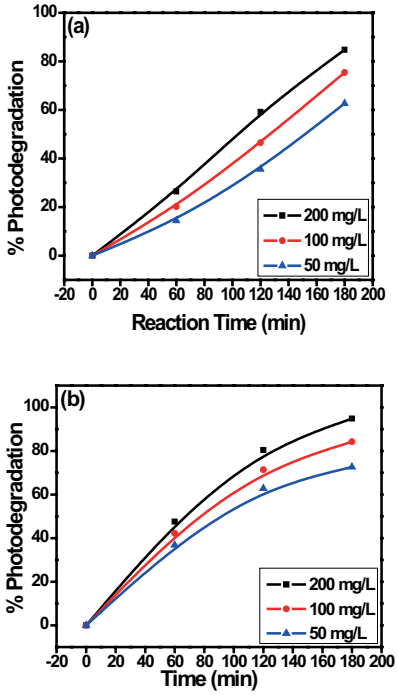

Fig. 11. Effect of dose on photodegradation of EBT: (a) TiO_2 and (b) Ni:TiO_2.

4.5. Recyclability of photocatalyst

The photocatalyst and EBT mixture were agitated, illuminated with visible light and after desired time, the mixture was centrifuge to remove the photocatalyst. The obtained photocatalyst was washed three times with distilled water and kept in oven for 24 h at 60°C and reused for the degradation of EBT. The photodegradation of EBT by the recyclized photocatalyst are showing in Figs. 12(a) and (b). The result shows that the recyclized photocatalyst efficiency is decreased probably due to the loss of some active sites and decrease of collection efficiency of photon.

4.6. GC–MS of EBT photodegradation products

The photodegradation of the EBT takes place by irradiating under visible light in the presence of bare TiO_2 and Ni-doped titania nanocomposite. The photodegraded products of photodegradation of EBT have been determined by GC–MS analysis (Figs. 13 and 15). It has been found that MS chromatograph (Figs. 14 and 16) and correspondingly mass chromatographs of EBT (after 2 h of irradiation) in the presence of bare TiO_2 and Ni:TiO_2 are almost similar, except in their respective intensities. Among the number of degraded products of EBT, seven products formed in the photodegradation, shown in mass chromatograph (Figs. 14 and 16) have been identified, as listed in Table 2. The mechanism for the photodegradation of EBT using titania nanocomposites is believed to take place by the photo produced e^- and h^+ that results into formation of highly oxidative species such as hydroxyl and superoxide radicals, which on reaction with EBT results into its decomposition to smaller molecules [45].

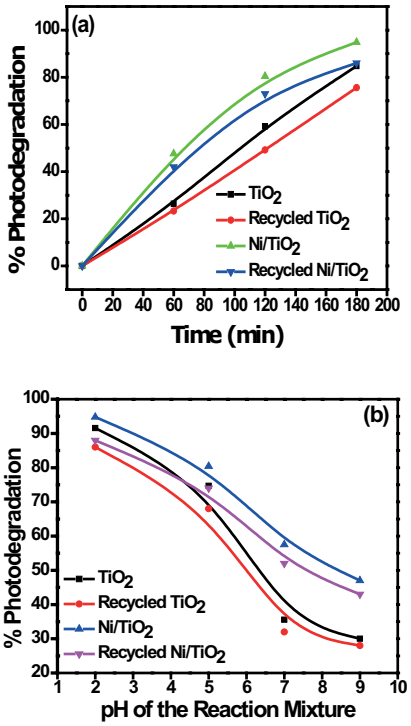

Fig. 12. Photodegradation of EBT by recyclable photocatalyst: (a) photodegradation with time and (b) photodegradation at different pH.

4.7. Lowering of electron–hole recombination

Photoluminescence spectra have been used to examine the mobility of the charge carriers to the surface as well as the recombination process involved by the electron–hole pairs in semiconductor particles. Photo lumiscence (PL) emission results from the radiative recombination of excited electrons and holes. In other words, it is a critical necessity of a good photocatalyst to have minimum electron–hole recombination. To study the recombination of charge carriers, PL studies of synthesized materials have been undertaken. PL emission intensity is directly related to recombination of excited electrons and holes. Fig. 17 shows the photoluminescence spectra of synthesized photocatalysts. In the PL spectra, the intensity of TiO_2 is higher than Ni:TiO_2 indicating rate of recombination of e^-–h^+ is higher in TiO_2 than that of Ni:TiO_2. The weak PL intensity of Ni:TiO_2 may arise due to the impregnation of Ni in titania lattice, which for sub-band level in band gap region of TiO_2. This delays the electrons–holes recombination process and hence utilized in the redox, reaction leading to improved photocatalytic activity [46].

4.8. Hydroxyl radical formation

As hydroxyl radical performs the key role for the decomposition of the organic pollutants, it is necessary to investigate the amount of hydroxyl radicals produced by each photocatalyst. In this study, terephthalic acid (TA) has been used as a probe reagent to evaluate •OH radical present in the photoreaction pathway. Fig. 18 shows the PL spectra of TiO_2 and Ni:TiO_2 recorded EBT solution in the presence of 10^{-3} M terephthalic solution. OH radical attack terephthalic, forming 2-hydroxyl terephthalic acid (TAOH) which gives a fluorescence signal at 426 nm [47]. The fluorescent intensity is linearly related to the number of hydroxyl radicals formed by the photocatalysts. Higher the generation of hydroxyl radical, more will be yield of TAOH and hence more intense will be the fluorescence peak. The spectra show that the intensity of peak indicating in the presence

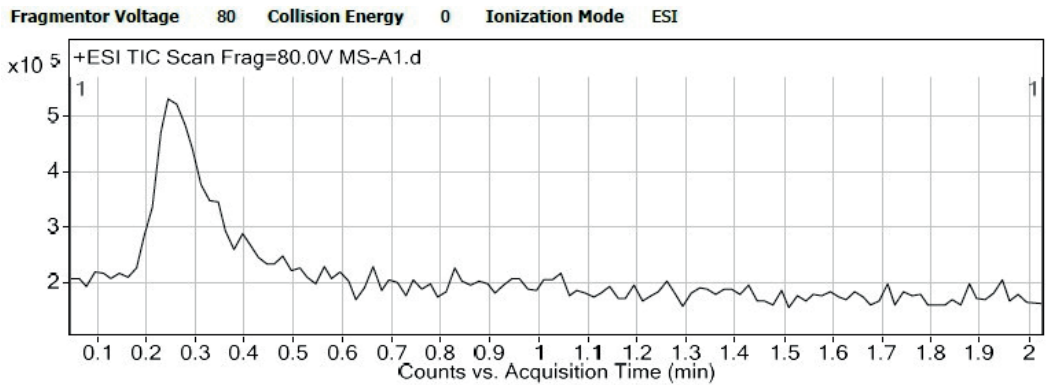

Fig. 13. GC chromatogram of EBT in presence of titania.

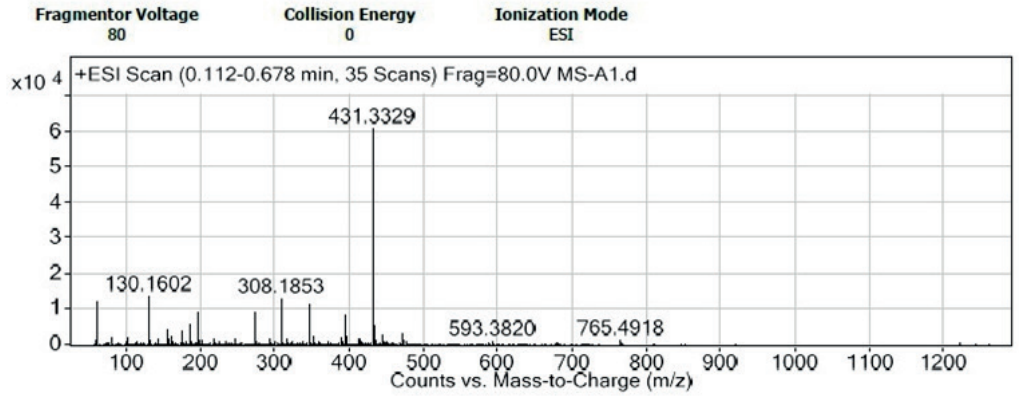

Fig. 14. Mass spectra of EBT photodegradation in presence of titania.

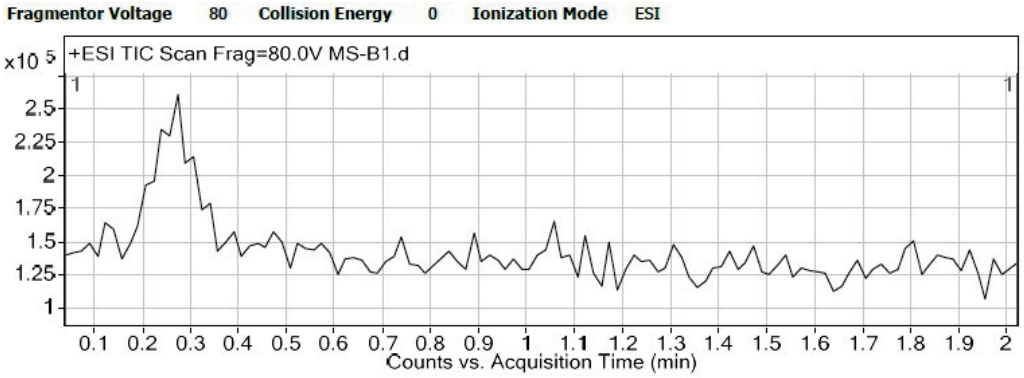

Fig. 15. GC chromatogram of EBT in presence of Ni:TiO_2.

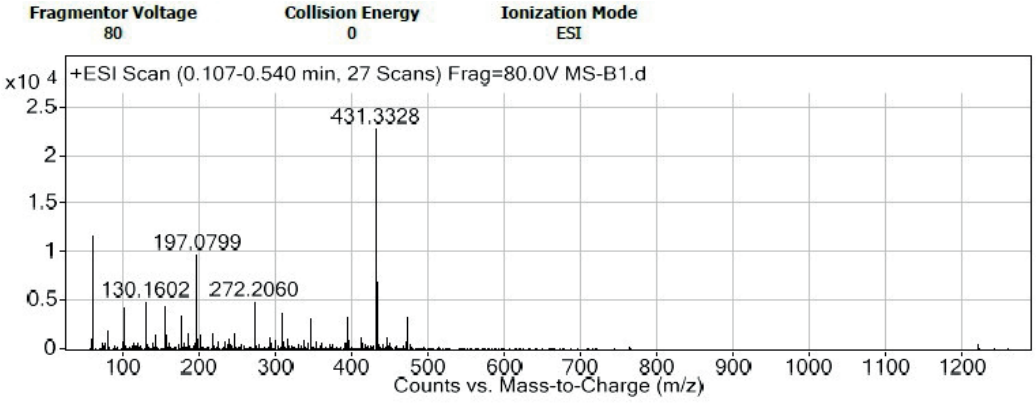

Fig. 16. Mass spectra of EBT photodegradation in presence of Ni:TiO_2.

of Ni:TiO_2 higher generation of more number of hydroxyl radicals compared with TiO_2.

5. Mechanism of photooxidation process

The acceleration of a chemical transformation by light in the presence of a catalyst is called photocatalysis. The catalyst may accelerate the photoreaction by interaction with the substrate in its ground or excited state and/or with a primary photoproduct, depending upon the mechanism of the photoreaction remaining unaltered at the end of each catalytic cycle. Heterogeneous photocatalysis is a process in which two active phases, solid and liquid are present. The solid phase is a catalyst, usually a semiconductor. The molecular orbital of semiconductors has a band structure. The bands of interest in photocatalysis are the populated VB and it is largely vacant CB, which is commonly characterized by band gap energy (E_{bg}). The semiconductors may be photoexcited to form electron-donor sites (reducing sites) and electron-acceptor sites (oxidising sites), providing great scope for redox reaction [48]. When the semiconductor is illuminated with light ($h\nu$) of greater energy than that of the

Table 2
Intermediate photoproducts formed during Eriochrome Black-T degradation by Ni:TiO_2 after 2 h visible light irradiation

S.No.	IUPAC name of compound	MS (*m*/*z*)
1	3-Hydroxy-7-nitroso-1,8 adihy-dronaphthalene-1-sulfonoperoxoic acid	272
2	2-(6-(Hydroxymethyl)-4-nitrocyclo-hexa-2,4-dienylidene)ethanol	197
3	2-Hydrazinylnaphthalen-1-ol	175
4	2-Diazenylnaphthalen-1-ol	155
5	4-Formylbenzonitrile	131
6	1-Ethynylbenzene	102
7	Methyl formate	60

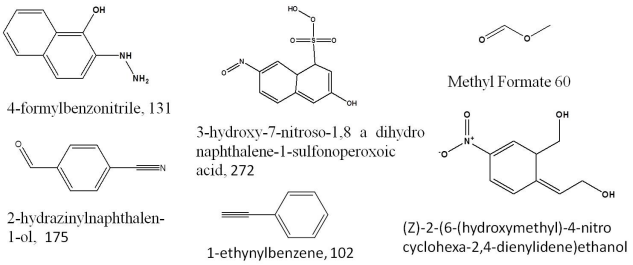

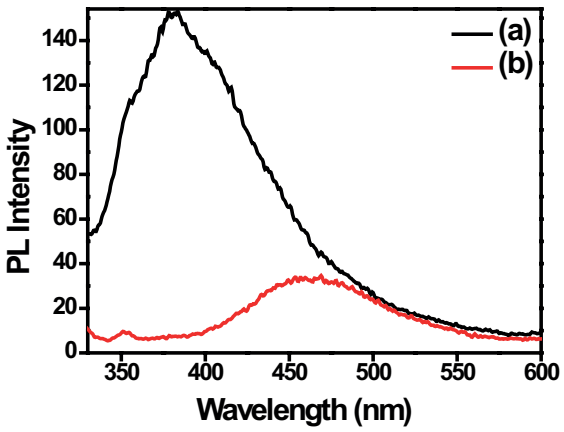

Fig. 17. Photolumiscence spectra of: (a) TiO_2 and (b) Ni:TiO_2.

band gap, an electron is promoted from the VB to the CB leaving a positive hole (h^+) in the VB and an electron (e^-) in the CB as illustrated in Fig. 19.

If charge separation is maintained, the electron and hole may migrate to the catalyst surface where they participate in redox reactions with sorbed species. Specially, h^+_{vb} may react with surface-bound H_2O or OH^- to produce the hydroxyl radical and e^-_{cb} is picked up by oxygen to generate superoxide radical anion (O_2^-), as indicated in the following Eqs. (6)–(8).

Absorption of efficient photons by titania ($h\upsilon \geq E_{bg}$ = 3.2 eV):

$$TiO_2 + h\upsilon \rightarrow e_{cb} + h^+_{vb} \quad (6)$$

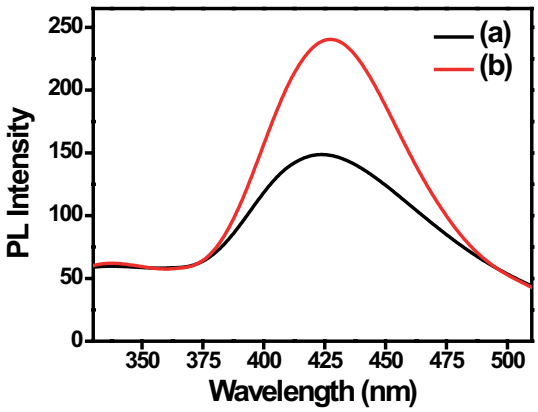

Fig. 18. PL spectra of photocatalyzed EBT solution in the presence of terephthalic acid (0.001 M) (a) TiO_2 and (b) Ni:TiO_2.

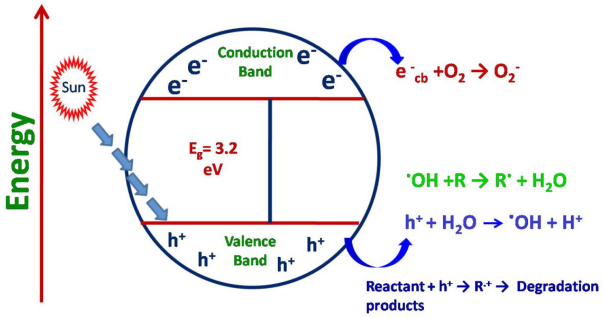

Fig. 19. Mechanism of photodegradation of titania and formation of free radical.

Formation of superoxide radical anion:

$$O_2 + e_{cb} \rightarrow O_2^- \quad (7)$$

Neutralization of OH^- group into OH by the hole:

$$(H_2O \Leftrightarrow H^+ + OH^-)_{ads} + h^+_{vb} \rightarrow {}^{\bullet}OH + H^+ \quad (8)$$

It has been suggested that the hydroxyl radical ($^{\bullet}OH$) and superoxide radical anions (O_2^-) are the primary oxidizing species in the photocatalytic oxidation processes. These oxidative reactions would result in the degradation of the pollutants as shown in the following Eqs. (9) and (10).

Oxidation of the organic pollutants via successive attack by OH radicals:

$$R + {}^{\bullet}OH \rightarrow R^{\bullet} + H_2O \quad (9)$$

or by direct reaction with holes:

$$R + h^+ \rightarrow R^{\bullet+} \rightarrow \text{degradation products} \quad (10)$$

For oxidation reactions to occur, the VB must have a higher oxidation potential than the material under consideration. The redox potential of the VB and the CB for different semiconductors varies between +4.0 and –1.5 V vs. normal

hydrogen electrode, respectively. The VB and CB energies of the TiO_2 are estimated to be +3.1 and –0.1 V, respectively, which means that its band gap energy is 3.2 eV, and therefore, absorbs in the near UV light ($\lambda < 387$ nm). Many organic compounds have a potential above that of the TiO_2 VB, and therefore, can be oxidized. In contrast, fewer organic compounds can be reduced since a smaller number of them have a potential below that of the TiO_2 CB.

6. Adsorption study

The degradation of EBT under visible light irradiation in the presence of TiO_2 and Ni:TiO_2 nanoparticles is an example of heterogeneous catalysis. Rate laws in such reactions seldom follow proper law model and hence are inherently more difficult to formulate from the data. It has been widely accepted that heterogeneous catalytic reactions can be analyzed with the help of Langmuir–Hinshelwood (LH) model [49,50], satisfying, the following assumptions: (i) there are limited number of adsorption sites on the catalyst and its surface is homogeneous, (ii) only one molecule can be adsorbed on one site and monolayer formation occurs, (iii) the absorption reaction is reversible in nature and (iv) the adsorbed molecules do not react amongst themselves [51]. According to LH model, following three steps take place in the kinetics mechanism [52], these steps are of adsorption, surface reaction and desorption of products from the surface.

Step 1: D (dye) + C (catalyst) → D·C (adsorption)
Step 2: D·C → E·C + other products (surface reaction)
Step 3: E·C → E + C (desorption)

The Freundlich isotherm [53] is employed, assuming a heterogeneous surface with a non-uniform distribution of heat of adsorption over the surface and it may be written as:

$$q_e = K_F C_e^{\frac{1}{n}} \tag{11}$$

The above equation can be linearized as:

$$\ln q_e = \ln K_F + \frac{1}{n}\ln C_e \tag{12}$$

where q_e (mg/g) is the amount of solute adsorbed per unit weight of adsorbent, C_e (mg/L) is the equilibrium concentration of solute, K_F (mg/g) is the Freundlich constant (which indicates the relative adsorption capacity of the adsorbent) and $1/n$ is the constant which indicates the intensity of adsorption. Since the TiO_2 is covered by both EBT as well as water molecules (C_{water}) by hydrogen bonding, their competition for the active sites cannot be ignored.

Langmuir adsorption model [54] can be applied to the aqueous solutions of dyes with the help of the following expression:

$$q = \frac{q_t}{q_{\max}} = \frac{K_L C}{1 + K_L C + K_{water} + C_{water}} \tag{13}$$

where q is the fractional sites covered by the dye, q_t is the absorbed quantity of dye at any time, $q_{\max}$ shows the maximum quantity of dye that can be adsorbed, K_L is the Langmuir adsorption constant for reactant and K_{water} is the adsorption constant for water. The value of $C_{water} >> C$, hence C_{water} remains almost same throughout the reaction and the catalyst coverage by water molecules remains almost constant. Thus, we can ignore the quantity K_{water}, C_{water} and rewrite Eq. (13) as:

$$q = \frac{K_L C}{1 + K_L C} \tag{14}$$

The quantity adsorbed at a particular time can also be expressed as:

$$qt = \frac{(\text{Reactor Volume}) \times (\text{Change in concentration})}{\text{Mass of catalyst}} \tag{15}$$

The equilibrium adsorption quantity q_{eq} can be written as:

$$q_e = q_{\max}\left(\frac{K_L C_e}{1 + K_L C_e}\right) \tag{16}$$

where C_e is the equilibrium concentration of the EBT. On transforming Eq. (16), a function can be derived as follows:

$$\frac{C_e}{q_e} = \frac{1}{K_L q_{\max}} + \frac{C_e}{q_{\max}} \tag{17}$$

The intercept on the vertical axis gives $1/K_L q_{\max}$ and the reciprocal of slope gives $q_{\max}$.

Fig. 20 indicates that the adsorption of EBT dye on the surface of Ni:TiO_2 follows the non-linear Freundlich adsorption isotherm. The Freundlich isotherm non-linear regression coefficient value was found to be 0.96 and Langmuir non-linear regression coefficient value was found to be 0.91 shown in Table 3. Therefore, the adsorption of dye EBT follows the Freundlich isotherm.

7. Kinetic study of photocatalytic degradation

For kinetic study of photocatalytic degradation, a control experiment was first carried out under two conditions namely (i) dye + visible light (no catalyst) and (ii) catalyst + dye in dark without any irradiation (Fig. 21). It can be seen that under dark conditions, the amount of catalyst adsorbed

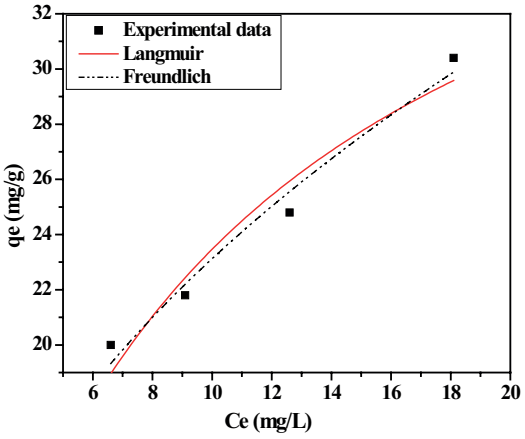

Fig. 20. Langmuir and Freundlich adsorption isotherm with experimental data for the EBT dye adsorption on Ni:TiO_2.

becomes constant after 20 min, where adsorption equilibrium is achieved (shown in Fig. 22). For kinetic study of bleaching of EBT, the initial concentration of the dyes was varied and the experiments were first conducted in dark for 20 min and then immediately followed by irradiation (Fig. 21). The amount of catalyst was kept constant (0.2 g) throughout the experiment.

Applying the LH model for determining the oxidation rate of the photocatalysis of dye:

$$\text{Rate}(r) = -\frac{dc}{dt} = k\theta = \theta = \frac{kK_AC}{1+K_AC} \tag{18}$$

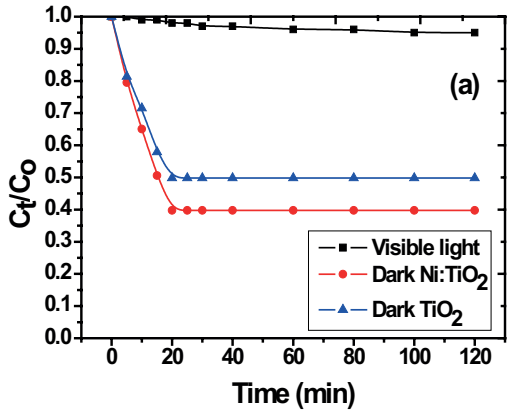

Fig. 21. Change in concentration under dark with TiO_2, Ni:TiO_2 and in visible light.

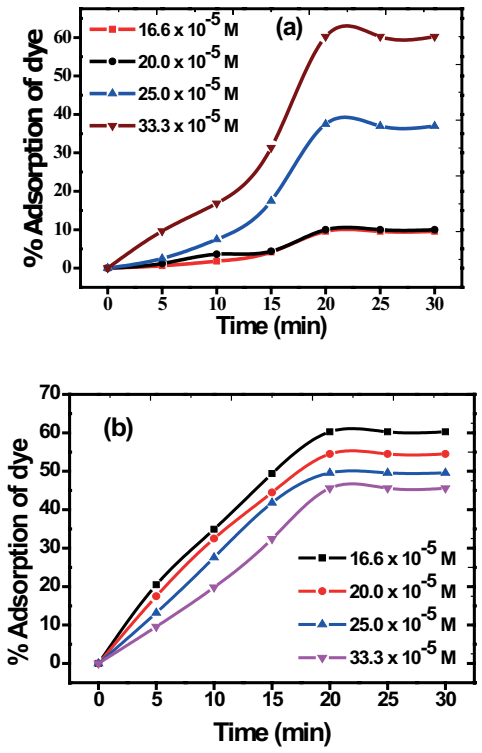

Fig. 22. Percentage adsorption under dark condition: (a) TiO_2 and (b) Ni:TiO_2.

where k is the rate constant (mg/L min^{-1}), C is the concentration of dye, K_A is the adsorption constant of the dye (L/mg) and t is the illumination time (min).

During the course of reaction, the initial pH, amount of catalyst and photointensity were kept same. In addition to it, the formation of intermediates may interfere in the rate determination; hence, the calculation was done at the beginning of irradiation. The rate expression can be written as:

$$r_0 = \frac{kK_AC_0}{1+K_AC_0} \tag{19}$$

where r_o is the initial rate of degradation of EBT and C_o is the initial concentration (almost equal to C_{eq}). When the initial concentration $C_{initial}$ is very small, C_o will also be small and Eq. (19) can be simplified as an first-order equation [55–58]:

$$-\frac{dc}{dt} = kK_AC_0 = \frac{\ln C_0}{C} = kK_At \tag{20}$$

$$C = C_0e^{-k_{f\,\text{photo}}t} \tag{21}$$

where $k_{f,\,\text{photo}} = kK_A$.

The value of $k_{f,\,\text{photo}}$ can be determined from the plot of $\ln C_t/C_o$ vs. t (Fig. 17). The slope of the straight line is the value of first-order rate constant (shown in Fig. 23) [59]. The value of apparent rate constant at various initial concentrations of dye solution for photocatalysis reaction in the presence of TiO_2 and Ni:TiO_2 are shown in Tables 4 and 5.

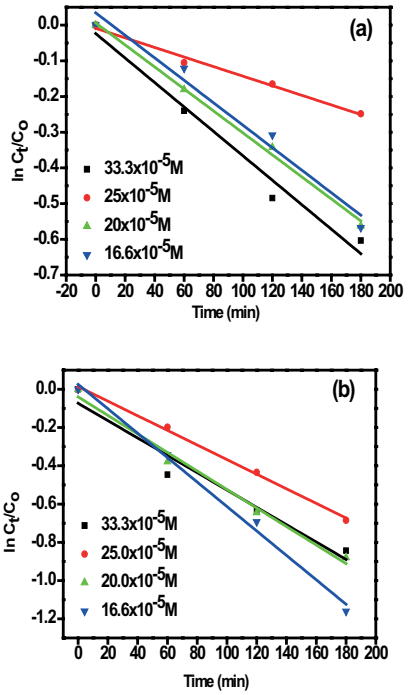

Fig. 23. Linear first-order reaction of Langmuir–Hinshelwood kinetics of EBT dye vs. time: (a) TiO_2 and (b) Ni:TiO_2 (initial concentration were 33.3, 25, 20, 16.6 × 10^{-5} M).

Table 3
Adsorption parameters of EBT adsorption

Adsorption equation	Isotherm parameter		R^2 (non-linear)
Freundlich	K_F	8.457	0.96
	$1/n$	0.432	
Langmuir	K_L	0.116	0.91
	q_{max}	43.62	

Table 4
Value of apparent rate constant at various initial concentrations of dye solution for photocatalysis reaction in the presence of TiO_2

Concentration (M)	k (min^{-1})	R^2
33.3×10^{-5}	–0.00342	0.96852
25.0×10^{-5}	–0.00304	0.98338
20.0×10^{-5}	–0.00308	0.99412
16.6×10^{-5}	–0.00315	0.96074

Table 5
Value of apparent rate constant at various initial concentrations of dye solution for photocatalysis reaction in the presence of Ni:-TiO_2

Concentration (M)	k (min^{-1})	R^2
33.3×10^{-5}	–0.004537	0.93066
25.0×10^{-5}	–0.003821	0.99589
20.0×10^{-5}	–0.004843	0.98083
16.6×10^{-5}	–0.006393	0.99086

The rate constant values for the photocatalytic degradation of EBT follow the first-order kinetic for the both photocatalyst. In case of TiO_2, the regression (R^2) coefficient values show large variation, and optimum value was obtained at 20.0×10^{-5} M concentration of dye, and in the case of Ni:TiO_2, the regression (R^2) coefficient values did not show variation whose optimum value was obtained at 25.0×10^{-5} M concentration of dye. This confirms that photocatalytic degradation of EBT follows first-order kinetic in the presence of TiO_2 and Ni:TiO_2.

8. Conclusion

In the present investigation, TiO_2 and Ni:TiO_2 nanoparticles were prepared and their photocatalytic degradation capacity was measured against of EBT under visible light irradiation. Prepared TiO_2 and Ni:TiO_2 nanoparticles were analyzed by XRD, SEM, TEM, UV–Vis, FTIR, BET and band gap energy. In the XRD pattern of TiO_2 and Ni:TiO_2 nanoparticles, both anatase and rutile phases were present. The particle size of TiO_2 and Ni:TiO_2 was calculated as 72 and 16 nm, respectively, using Scherrer's equation. SEM and TEM images of TiO_2 and Ni:TiO_2 nanoparticles were found as agglomerate in nanometric dimension. The doping of Ni^{2+} indicates that the particle size reduces due to the penetration of nickel in the lattice of TiO_2. Doping with 5% Ni, the crystallite size was decreased and the surface area value increased. These results suggest that Ni doping effectively inhibits TiO_2 grain growth probably by staying at grain boundaries thereby decreasing the crystallite size and increasing the surface area. The undoped TiO_2 showed absorbance in the shorter wavelength region while Ni:TiO_2 results showed slight red shift in the absorption edge. The band gap energy E_g value of TiO_2 and Ni:TiO_2 was found to be 3.2 and 3.0 eV, respectively. The slight decrease in band gap energy in case of Ni:TiO_2 is due to the formation of sub-band level between VB and CB due to doping of Ni^{2+} in TiO_2 host. The broad intense band below 820, 804, 592 and 456 cm^{-1} is due to Ti–O–Ti vibrations and Ni:TiO_2 shows strong band at 1,075 cm^{-1}, corresponds to the vibration of Ni–O bond and confirms the penetration of nickel in titania. The photodegradation of EBT was investigated at different condition of concentration and pH in the presence of TiO_2 and Ni:TiO_2. The effective photodegradation of EBT was found better in the presence of Ni:TiO_2 than the pure TiO_2. •OH radicals mediated photocatalytic degradation of EBT was proved by GC–MS. Since TA is readily converted to TAOH in the presence of •OH radical, the photolumiscence spectra of photodegraded EBT with TA shows higher photolumiscence peak correspond to TA in the presence of Ni:TiO_2 than TiO_2. Photodegradation of EBT is following the pseudo-first-order kinetics. Complete degradation of EBT was more prominent in 180 min, in the presence of Ni:TiO_2 while it was 90% in the presence of TiO_2 in same condition.

Acknowledgements

The author would like to thank UGC, Government of India, for financial assistance. The authors also acknowledge the support provided by the Babasaheb Bhimrao Ambedkar University, Lucknow, India.

References

[1] A.A. Ahmad, B.H. Hameed, N. Aziz, Adsorption of direct dye on palm ash: kinetic and equilibrium modeling, J. Hazard. Mater., 141 (2007) 70–76.
[2] N. Barka, A. Assabbane, A. Nounah, L. Laanab, Y.A. Ichou, Removal of textile dyes from aqueous solutions by natural phosphate as a new adsorbent, Desalination, 235 (2009) 264–275.
[3] N. Barka, S. Qourzal, A. Assabbane, A. Nounah, Y.A. Ichou, Adsorption of Disperse Blue SBL dye by synthesized poorly crystalline hydroxyapatite, J. Environ. Sci., 20 (2008) 1268–1272.
[4] D.V. Bavykin, K.E. Redmond, B.P. Nias, A.N. Kulak, F.C. Walsh, The effect of ionic charge on the adsorption of organic dyes onto titanate nanotubes, Aust. J. Chem., 63 (2010) 270–275.
[5] M.I. Franch, J. Peral, X. Domènech, R.F. Howe, J.A. Ayllón, Enhancement of photocatalytic activity of TiO_2 by adsorbed aluminium(III), Appl. Catal., B, 55 (2005) 105–113.
[6] W.T. Tsai, C.Y. Chang, M.C. Lin, S.F. Chien, H.F. Sun, M.F. Hsieh, Adsorption of acid dye onto activated carbons prepared from agricultural waste bagasse by $ZnCl_2$ activation, Chemosphere, 45 (2001) 51–58.
[7] H. Kono, R. Kusumoto, Removal of anionic dyes in aqueous solution by flocculation with cellulose ampholytes, J. Water Process Eng., 7 (2015) 83–93.
[8] R. Gong, S. Zhu, D. Zhang, J. Chen, S. Ni, R. Guan, Adsorption behavior of cationic dyes on citric acid esterifying wheat straw: kinetic and thermodynamic profile, Desalination, 230 (2008) 220–228.
[9] N.K. Goel, V. Kumar, N. Misra, L. Varshney, Cellulose based cationic adsorbent fabricated via radiation grafting process for treatment of dyes waste water, Carbohydr. Polym., 132 (2015) 444–451.

[10] S. Wijannarong, S. Aroonsrimorakot, P. Thavipoke, C. Kumsopa, S. Sangjan, Removal of reactive dyes from textile dyeing industrial effluent by ozonation process, APCBEE Procedia, 5 (2013) 279–282.
[11] H. Laguna, S. Loera, I.A. Ibarra, E. Lima, M.A. Vera, V. Lara, Azoic dyes hosted on hydrotalcite-like compounds: non-toxic hybrid pigments, Microporous Mesoporous Mater., 98 (2007) 234–241.
[12] N. Hirun, V. Tantishaiyakul, W. Pichayakorn, Effect of Eriochrome Black T on the gelatinization of xyloglucan investigated using rheological measurement and release behavior of Eriochrome Black T from xyloglucan gel matrices, Int. J. Pharm., 388 (2010) 196-201
[13] H. Song, C. Chen, H. Zhang, J. Huang, Rapid decolorization of dyes in heterogeneous Fenton-like oxidation catalyzed by Fe-incorporated Ti-HMS molecular sieves, J. Environ. Chem. Eng., 4 (2016) 460–467.
[14] K. Chinoune, K. Bentaleb, Z. Bouberka, A. Nadim, U. Maschke, Adsorption of reactive dyes from aqueous solution by dirty bentonite, Appl. Clay Sci., 123 (2016) 64–75.
[15] E. Rubin, P. Rodriguez, R. Herrero, J. Cremades, I. Barbara, M.E.S. de Vicente, Removal of Methylene Blue from aqueous solutions using as biosorbent *Sargassum muticum*: an invasive macroalga in Europe, J. Chem. Technol. Biotechnol., 80 (2005) 291–298.
[16] C.L. Porras, A.T. Teran, O.V. Becerra, M.M. Yoshida, M.R. Villalobos, M.G. Guaderrama, J.A. Martínez, Low-temperature synthesis and characterization of anatase TiO_2 nanoparticles by an acid assisted sol-gel method, J. Alloys Compd., 647 (2015) 627–636.
[17] H. Cai, W. Mu, W. Liu, X. Zhang, Y. Deng, Sol–gel synthesis highly porous titanium dioxide microspheres with cellulose nanofibrils-based aerogel templates, Inorg. Chem. Commun., 51 (2015) 71–74.
[18] O. Jongprateep, R. Puranasamriddhi, J. Palomas, Nanoparticulate titanium dioxide synthesized by sol–gel and solution combustion techniques, Ceram. Int., 41 (2015) S169–S173.
[19] H. Lee, Y.K. Park, S.J. Kim, B.H. Kim, S.C. Jung, Titanium dioxide modification with cobalt oxide nanoparticles for photocatalysis, J. Ind. Eng. Chem., 32 (2015) 259–263.
[20] H. Jia, Z. Zheng, H. Zha, L. Zhang, Z. Zou, Non-aqueous sol–gel synthesis and growth mechanism of single crystalline TiO_2 nanorods with high photocatalytic activity, Mater. Res. Bull., 44 (2009) 1312–1316.
[21] M.N. Makwana, J.T. Christopher, I.G. Robert, P.F. McMillan, Pilot plant scale continuous hydrothermal synthesis of nano-titania; effect of size on photocatalytic activity, Mater. Sci. Semicond. Process., 42 (2016) 131–137.
[22] C.M. Ng, P.C. Chen, S. Manickam, Hydrothermal crystallization of titania on silver nucleation sites for the synthesis of visible light nano-photocatalysts—enhanced photoactivity using Rhodamine 6G, Appl. Catal., A, 433–434 (2012) 75–80.
[23] A. Gananaprakasam, V.M. Sivakumar, P.L. Sivayogavalli, M.T. Murugan, Characterization of TiO_2 and ZnO nanoparticles and their applications in photocatalytic degradation of azodyes , Ecotoxicol. Environ. Saf., 121 (2015) 121–125.
[24] S. Kaur, V. Singh, Visible light induced sonophotocatalytic degradation of Reactive Red dye 198 using dye sensitized TiO_2, Ultrason. Sonochem., 14 (2007) 531–537.
[25] L. Cavigli, F. Bogani, A. Vinattieri, V. Faso, G. Baldi, Volume versus surface-mediated recombination in anatase TiO_2 nanoparticles, J. Appl. Phys., 106 (2009) 053516.
[26] S. Liu, N. Jaffrezic, C. Guillard, Size effects in liquid-phase photo-oxidation of phenol using nanometer-sized TiO_2 catalysts, Appl. Surf. Sci., 255 (2008) 2704–2709.
[27] M. Scarisoreanu, I. Morjan, R. Alexandrescu, C.T. Fleaca, A. Badoi, E. Dutu, A.-M. Niculescu, C. Luculescu, E. Vasile, J. Wang, S. Bouhadoun, N. Herlin-Boime, Enhancing the visible light absorption of titania nanoparticles by S and C doping in a single-step process, App. Surf. Sci., 302 (2014) 11–18.
[28] E. Baran, B. Yazici, Effect of different nano-structured Ag doped TiO_2-NTs fabricated by electrodeposition on the electrocatalytic hydrogen production, Int. J. Hydrogen Energy, 41 (2016) 2498–2511.
[29] B. Choudhury, M. Dey, A. Choudhury, Defect generation, *d-d* transition, and band gap reduction in Cu-doped TiO_2 nanoparticles, Int. Nano Lett., 3 (2013) 25.
[30] A.E. Gary, C. Lin, Investigation of retardation effects on the titanium dioxide photodegradation system, Chemosphere, 46 (2002) 937–944.
[31] M. Toyoda, T. Yano, B. Tryba, S. Mozia, T. Tsumura, M. Inagaki, Preparation of carbon-coated Magneli phases Ti_nO_{2n-1} and their photocatalytic activity under visible light, Appl. Catal., B, 88 (2009) 160–164.
[32] R. Byberg, J. Cobb, L.D. Martin, R.W. Thompson, T.A. Camesano, O. Zahraa, M.N. Pons, Comparison of photocatalytic degradation of dyes in relation to their structure, Environ. Sci. Pollut. Res., 20 (2013) 3570–3581.
[33] R. Matos, E. Montan, V. Rivero, Influence of activated carbon upon the photocatalytic degradation of methylene blue under UV–Vis irradiation, Environ. Sci. Pollut. Res., 22 (2015) 784–791.
[34] B. Pal, R. Kaur, I.S. Grover, Superior adsorption and photodegradation of eriochrome black-T dye by Fe^{3+} and Pt^{4+} impregnated TiO_2 nanostructures of different shapes , J. Ind. Eng. Chem., 33 (2016) 178–184.
[35] B.D. Cullity, S.R. Stock, Elements of X-Ray Diffraction, 3rd ed., Prentice-Hall, Inc., New Jersey, 2001.
[36] A. Kumar, G. Hitkari, S. Singh, M. Gautam, G. Pandey, Synthesis of Ni:TiO_2 nanocomposites and photocatalytic degradation of oxalic acid in waste water, Int. J. Innov. Res. Sci. Eng. Technol., 4 (2015) 12721–12731.
[37] A. Kumar, G. Hitkari, M. Gautam, S. Singh, G. Pandey, Synthesis, characterization and application of Cu-TiO_2 nanaocomposites in photodegradation of Methyl Red (MR), Int. Adv. Res. J. Sci. Eng. Technol., 2 (2015) 50–55.
[38] A. Fujishima, K. Honda, Electrochemical photolysis of water at a semiconductor electrode, Nature, 238 (1972) 37–38.
[39] K. Madhusudan Reddy, S.V. Manorama, A. Ramachandra Reddy, Bandgap studies on anatase titanium dioxide nanoparticles, Mater. Chem. Phys., 78 (2002) 239–245.
[40] R.Q. Cabrera, A. Mills, C.R. O'Rourke, Action spectra of P25 TiO_2 and a visible light absorbing, carbon modified titania in the photocatalytic degradation of stearic acid, Appl. Catal., B, 150–151 (2014) 338–344.
[41] R.W. Matthews, Kinetics of photocatalytic oxidation of organic solutes over titanium dioxide, J. Catal., 111 (1988) 264–272.
[42] M. Vautier, C. Guillard, J.M. Herrmann, Photocatalytic degradation of dyes in water: case study of Indigo and of Indigo Carmine, J. Catal., 201 (2001) 46–59.
[43] S. Yang, X. Yang, X. Shao, R. Niu, L. Wang, Activated carbon catalyzed persulfate oxidation of azo dye acid orange 7 at ambient temperature, J. Hazard. Mater., 186 (2011) 659–666.
[44] H. Lachheb, E. Puzenat, A. Houas, M. Ksibi, E. Elaloui, C. Guillard, J.M. Herrmann, Photocatalytic degradation of various types of dyes (Alizarin S, Crocein Orange G, Methyl Red, Congo Red, Methylene Blue) in water by UV-irradiated titania, Appl. Catal., B, 39 (2002) 75–90.
[45] G.A. Epling, C. Lin, Photoassisted bleaching of dyes utilizing TiO_2 and visible light, Chemosphere, 46 (2002) 561–570.
[46] S. Babu, A. Velez, K. Wozniak, J. Szydlowska, S. Seal, Electron paramagnetic study on radical scavenging properties of ceria nanoparticles, Chem. Phys. Lett., 442 (2007) 405–408.
[47] M.M. Ba-Abbad, A.A.H. Kadhum, A.B. Mohamad, M.S. Takriff, K. Sopian, Synthesis and catalytic activity of TiO_2 nanoparticles for photochemical oxidation of concentrated chlorophenols under direct solar radiation, Int. J. Electrochem. Sci., 7 (2012) 4871–4888.
[48] I.K. Konstantinou, T.A. Albanis, TiO_2-assisted photocatalytic degradation of azo dyes in aqueous solution: kinetic and mechanistic investigations: a review, Appl. Catal., B, 49 (2004) 1–14.
[49] M. Hema, A.Y. Arasi, P. Tamilselvi, R. Anbarasan, Titania nanoparticles synthesized by sol–gel technique, Chem. Sci. Trans., 2 (2013) 239–245.
[50] A.Y. Nosaka, J. Nishino, T. Fujiwara, T. Ikegami, H. Yagi, H. Akutsu, Y. Nosaka, Effects of thermal treatments on the recovery of adsorbed water and photocatalytic activities of TiO_2 photocatalytic systems, J. Phys. Chem. B, 110 (2006) 8380–8385.

[51] P. Singh, M.C. Vishnu, K.K. Sharma, A. Borthakur, P. Srivastava, D.B. Pal, D. Tiwary, P.K. Mishra, Photocatalytic degradation of Acid Red dye stuff in the presence of activated carbon-TiO_2 composite and its kinetic enumeration, J. Water Process Eng., 12 (2016) 20–31.
[52] E. Vulliet, J.M. Chovelon, C. Guillard, J.M. Herrmann, Factors influencing the photocatalytic degradation of sulfonylurea herbicides by TiO_2 aqueous suspension, J. Photochem. Photobiol., A, 159 (2003) 71–79.
[53] N. Guetta, H.A. Amar, Photocatalytic oxidation of methyl orange in presence of titanium dioxide in aqueous suspension. Part II: Kinetics study, Desalination, 185 (2005) 439–448.
[54] D. Chen, A.K. Ray, Photocatalytic kinetics of phenol and its derivatives over UV irradiated TiO_2, Appl. Catal., B, 23 (1999) 143–157.
[55] H. Freundlich, On the adsorption in solutions, J. Phys. Chem., 57 (1907) 385–470.
[56] I. Langmuir, The adsorption of gases on plane surfaces of glass, mica and platinum, J. Am. Chem. Soc., 40 (1918) 1361–1403.
[57] A.R. Biris, D. Toloman, A. Popa, M. D. Lazar, G.K. Kannarpady, V. Saini, F. Watanabe, B.P. Chhetri, A. Ghosh, A.S. Biris, Synthesis of tunable core–shell nanostructures based on TiO_2-graphene architectures and their application in the photodegradation of Rhodamine dyes, Physica E Low Dimens. Syst. Nanostruct., 81 (2016) 326–333.
[58] A. Zaleska, J.W. Sobczak, E. Grabowska, J. Hupka, Preparation and photocatalytic activity of boron-modified TiO_2 under UV and visible light, Appl. Catal. B, 78 (2008) 92–100.
[59] X.Z. Li, F.B. Li, C.L. Yang, W.K. Ge, Photocatalytic activity of WOx-TiO_2 under visible light irradiation, J. Photochem. Photobiol., A, 141 (2001) 209–217.